A Thorough Analysis of Various Geometries for a Dynamic Calibration Target for Through-wall and Through-rubble Radar

Michael J. Harner[a], Ram M. Narayanan[a], John R. Jendzurski[b], and Nicholas G. Paulter[b]

[a]Dept. of Electrical Engineering, The Pennsylvania State Univ., University Park, PA 16802
[b]National Institute of Standards and Technology, 100 Bureau Dr, Gaithersburg, MD 20899

ABSTRACT

It is common practice to use a metal conducting sphere for radar calibration purposes. The aspect-independence of a sphere allows for a more accurate and repeatable calibration of a radar than using a nonspherical calibration artifact. In addition, the radar cross section (RCS) for scattering spheres is well-known and can be calculated fairly easily using far field approximations. For Doppler radar testing, it is desired to apply these calibration advantages to a dynamic target. To accomplish this, a spherical polyhedron is investigated as the calibration target. This paper analyzes the scattering characteristics for various spherical polyhedral geometries. Each geometry is analyzed at 3.6 GHz in two states: contracted and expanded. For calibration purposes, it is desired that the target have a consistent monostatic RCS over the entirety of its surface. The RCS of each spherical polyhedral is analyzed and an optimized geometry, for calibration purposes, is chosen.

Keywords: RCS, calibration, monostatic, through-wall, through-rubble, human respiration, heartbeat, radar

1. INTRODUCTION

Through-wall and through-rubble Doppler radar has proven to be a very effective tool for human detection. It has become popular within the military and law enforcement, where through-wall sensing can locate the enemy and help to diffuse a hostile situation. It has found its niche in natural disaster events as well, where survivors buried deep under mounds of rubble can be detected and brought to safety. As the technology behind these radar systems continues to evolve, there continues to be a need for accurate, human-like calibration targets that can be used for the testing and optimization of these systems.[1]

The ideal calibration target offers simplicity in its usage as well as an identical scattering profile to that of a human. This is achievable if the following two characteristics are attained: (1) the radar cross section (RCS) of the target is nominally equivalent to that of a human and (2) the RCS of the target at all viewing angles remains relatively constant. In Doppler radar testing, the target's RCS will largely impact the radar's ability to distinguish between that target and the ambient noise around it. If the calibration target's RCS is too low, the target may be undetectable. If the RCS is too high, the radar receiver front-end may be driven into saturation. Both of these circumstances could result in a radar system being improperly tuned for human detection. For this reason, it is of great importance that the calibration target resemble the radar cross section of a human. This was stated in Ref. [2]. It is likely that a through-barrier calibration target would be placed in rugged conditions (e.g. immersed in a rubble pit) during testing. In such a setting, the target is likely to move and rotate which could be detrimental to the calibration process if its RCS is aspect-dependent.

An ideal geometry for the calibration target that would satisfy both requirements (1 and 2) is the perfect electrical conductor (PEC) sphere. PEC spheres have long been used for calibration due to some of their unique properties. The most useful of these properties is the sphere's ability to possess aspect independence. No matter from which direction the sphere is illuminated, it will have the same monostatic RCS. This is significant because

Further author information: (Send correspondence to M.J.H.)
M.J.H.: E-mail: mjh5681@yahoo.com

it greatly simplifies the calibration procedure; a slight tilt or misalignment will not have any impact. The sphere is also unique in that its exact RCS is well-known and easily calculable. When operating in the optical region (i.e., when the radius is much larger than the radar wavelength), the RCS is simply a function of its size. This property allows the calibration target to be properly scaled so that the RCS matches that of a human.

Since the calibration target is tailored for human sensing Doppler radar, it is paramount that the sphere be dynamic and capable of mimicking human physiological motion associated with heartbeat and respiration. This can be done by dividing the sphere into multiple parts, thus forming a spherical polyhedron. Each section of the polyhedron can then be controlled separately via linear actuators. As the actuators push and pull in unison, the polyhedron resembles a sphere repeatedly expanding and contracting. After proper dimensioning of the target, these oscillatory movements will bear resemblance to a human torso's movements, such as respiration and heartbeat. The target must maintain aspect independence at every viewing angle, however. However, the gaps that form when each section of the sphere moves radially to the expanded state may cause the desired aspect independence to be compromised because of the electrical discontinuities of the gaps. For this reason, various polyhedra were analyzed to determine the optimal number of sections. The electromagnetic simulations were performed using a transmit frequency of 3.6 GHz, which is representative of frequencies used in through-barrier radar systems. In the following sections, we discuss our findings and select a polyhedron that we feel possesses sufficient potential as a through-wall and through-rubble human sensing Doppler radar calibration target.

2. EMULATING HUMAN RCS

The RCS of a human's torso is largely related to his/her body characteristics. The natural variation in human body types causes a wide variation in RCS distribution over a population. Such characteristics include height, weight, and body fat composition. The RCS difference between a small child and an adult is significant. When weighing all of these factors, it was clear that more than one calibration target would be needed to represent multiple body compositions. For the time being, our goal was to focus on one body type and find an optimal architecture for our calibration target. There is significant literature in regards to using respiratory motion for human detection via Doppler radar systems.[2–6] One of the major areas of interest is in finding human RCS due solely to respiration and heartbeat movements on the torso; this excludes other parts of the body such as arms, legs, and head. In Ref. [7], this is coined as effective radar cross section (ERCS). They examined a group of 20 participants that took part in an ERCS analysis.[7] Using medical statistics from Ref. [8] we were able to pinpoint a participant who best-resembled the average American male in terms of height, weight, and body mass index (BMI). According to the Kiriazi study, the ERCS of the average American male was 0.249 m^2 in the prone position. This number gave us a reasonable guideline for designing our calibration target. Our target RCS, as mentioned in the next section, lies around this value.

3. ANALYZING VARIOUS GEOMETRIES

We analyzed the following five geometries: (1) spherical tetrahedron, (2) spherical hexahedron, (3) spherical octahedron, (4) spherical dodecahedron, and (5) spherical icosahedron. Each geometry was simulated twice; once in its contracted state and once in its expanded state. Each geometry was constructed so that the target approximately resembled a PEC sphere whilst in the contracted state. In this state, the diameter of the target was 50 cm. In the expanded state, each face was radially displaced 10 mm, based on a typical chest expansion after inhalation. The faces of the sphere were constructed to be 2 mm thick. In the contracted state, we implemented a small radial displacement of 0.2 mm. This is so that very small electrical discontinuities would exist between the faces, as they would in reality, despite the sphere being in a contracted state. For both states, the target operates in the optical region which allows us to estimate the theoretical RCS using the far field approximation, πa^2.[9] The expected RCS for a PEC sphere in the contracted and expanded state is computed as 0.196 m^2 and 0.204 m^2, respectively. We expect the target to slightly vary from a PEC sphere, however, due to the electrical discontinuities. Each simulation was run in the far field at 3.6 GHz. A Physical Optics (PO) solver was used. The simulation results are shown graphically in a three-dimensional format. The most important characteristic in these results is aspect independence. Ideally, a geometry will possess a constant RCS over its entire surface whilst expanded.

3.1 Spherical Tetrahedron

The first geometry shown is the four-sided tetrahedron. The monostatic RCS results are given in Figures 1 and 2 and for the contracted and expanded positions, respectively. In the contracted state, the target's RCS appears constant over the entirety of the surface. The simulation results show an RCS of approximately 0.20 m^2 which is consistent with the theoretical approximation. As expected, much of the RCS consistency is lost in the expanded state due to the gaps that come about. We believe that the higher RCS levels are likely due to plane waves traveling between the gaps, reflecting off of the inside, and interfering constructively on the path back towards the radar. These bright spots on the target could have an unwanted impact on the data collection process.

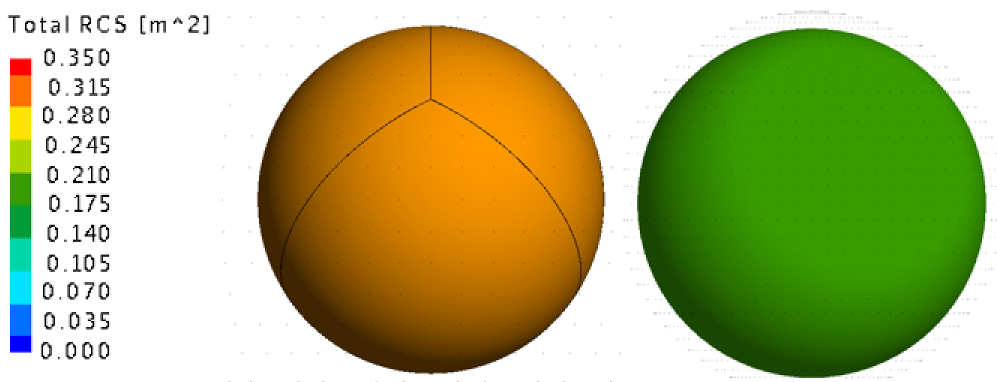

Figure 1. Monostatic RCS results of the tetrahedron in the contracted state at 3.6 GHz. The image of the target is shown on the left and its RCS simulation results on the right.

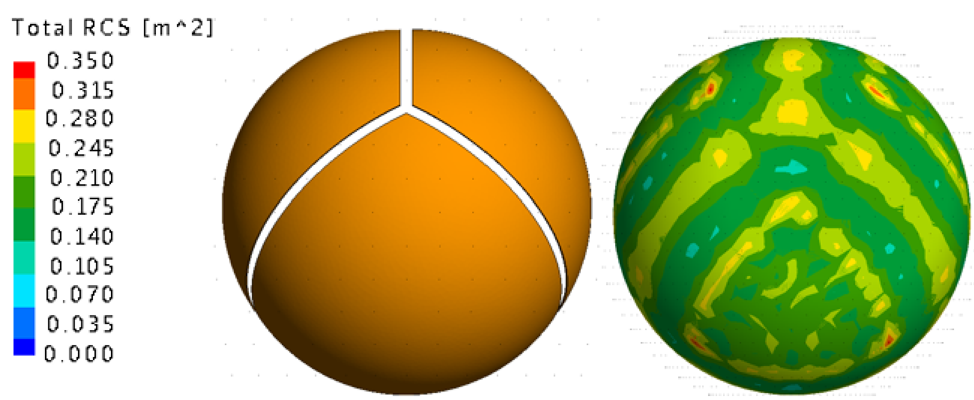

Figure 2. Monostatic RCS results of the tetrahedron in the expanded state at 3.6 GHz. The image of the target is shown on the left and its RCS simulation results on the right.

3.2 Spherical Hexahedron

The second geometry analyzed is the six-sided hexahedron. The monostatic RCS results are given in Figures 3 and 4 for the contracted and expanded positions, respectively. Again, there is great RCS consistency in the contracted state with numbers close to that of the theoretical approximation. The expanded state shows much less consistency in RCS, but the variability of the RCS over the surface is less than for the four-sided polyhedron. For example, most of the variance in RCS is between 0.175 m^2 and 0.260 m^2. Although this is not ideal, it is encouraging that the range in RCS values (i.e. variance) are mostly within a small window. Unfortunately, higher RCS values approaching 0.35 m^2 are once again seen in small areas on the sphere; concentrated mostly around the center of the face.

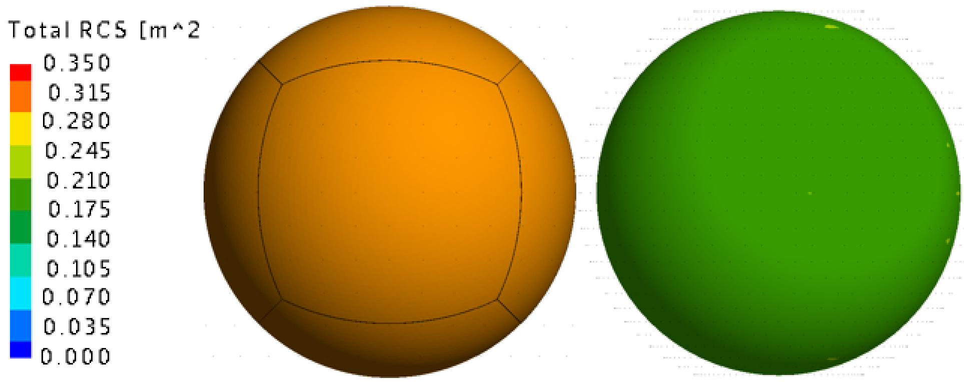

Figure 3. Monostatic RCS results of the hexahedron in the contracted state at 3.6 GHz. The image of the target is shown on the left and its RCS simulation results on the right.

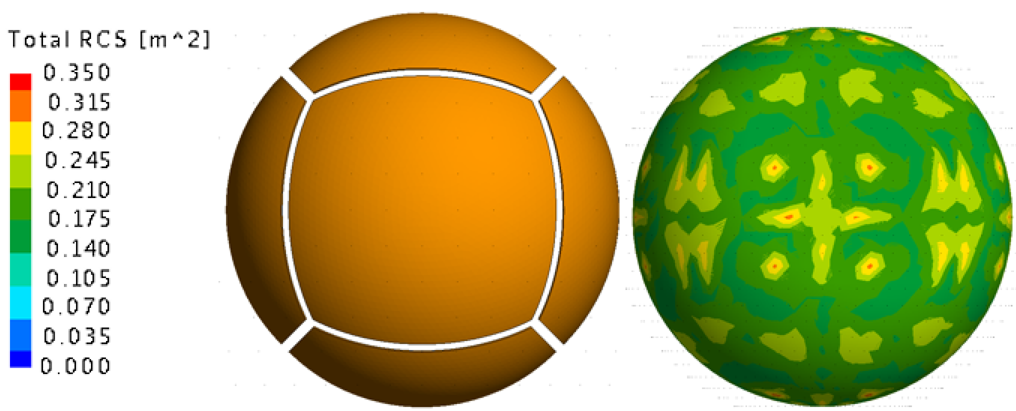

Figure 4. Monostatic RCS results of the hexahedron in the expanded state at 3.6 GHz. The image of the target is shown on the left and its RCS simulation results on the right.

3.3 Spherical Octahedron

The third geometry shown is the eight-sided octahedron. The monostatic RCS results are given in Figures 5 and 6 for the contracted and expanded positions, respectively. Once again, the RCS remains very consistent when the target is in its contracted state. The octahedron also shows better RCS consistency in its expanded state than the tetrahedron and hexahedron. The variance in RCS is small similar to that of the hexahedron. Although there are a few high-RCS values that exist towards the center of the faces, they appear to be a smaller quantity compared to the hexahedron.

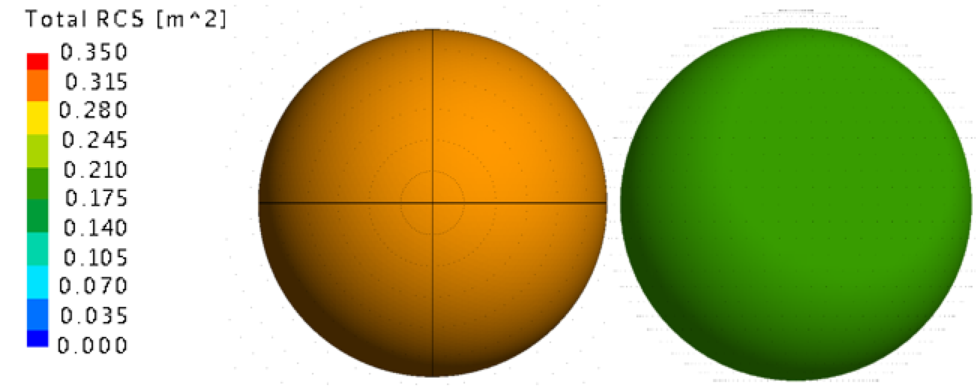

Figure 5. Monostatic RCS results of the octahedron in the contracted state at 3.6 GHz. The image of the target is shown on the left and its RCS simulation results on the right.

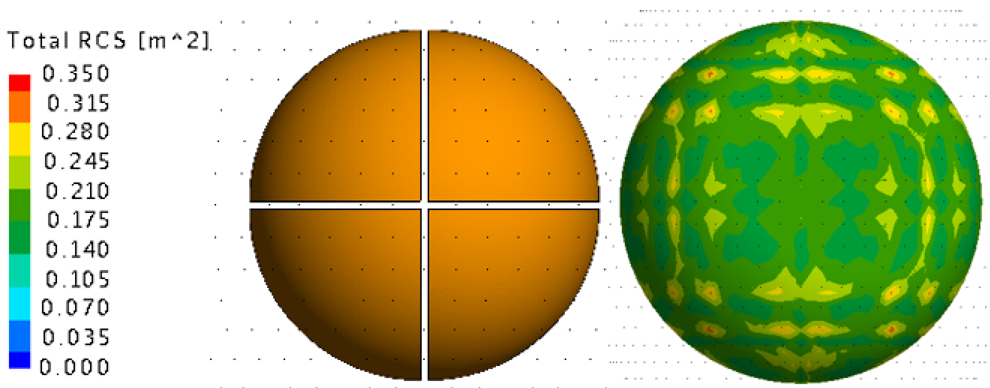

Figure 6. Monostatic RCS results of the octahedron in the expanded state at 3.6 GHz. The image of the target is shown on the left and its RCS simulation results on the right.

3.4 Spherical Dodecahedron

The monostatic RCS results for the dodecahedron are given in Figures 7 and 8 for the contracted and expanded positions, respectively. The dodecahedron possesses great RCS consistency while contracted, but a large amount of inconsistency when expanded. A clear pattern can be seen where bright spots exist at the center of each pentagonal face as well as at intersections where three faces intersect.

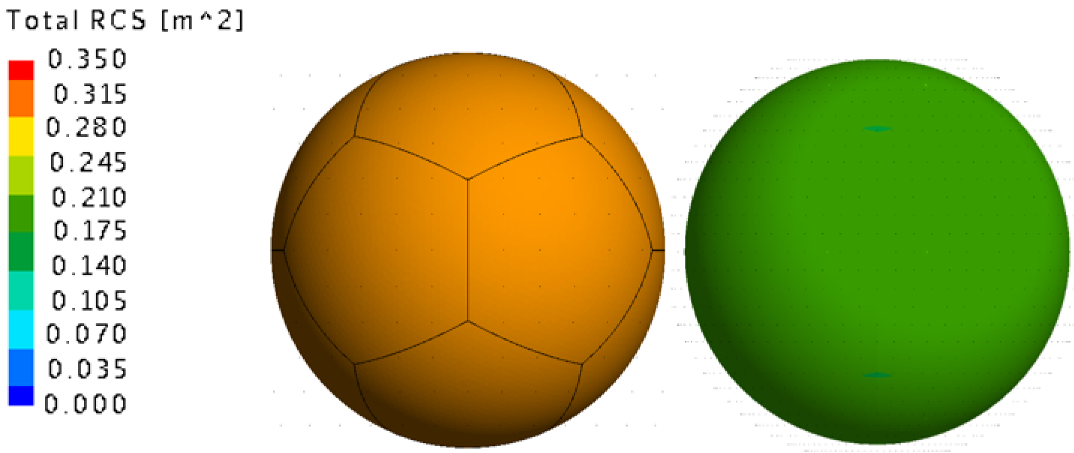

Figure 7. Monostatic RCS results of the dodecahedron in the contracted state at 3.6 GHz. The image of the target is shown on the left and its RCS simulation results on the right.

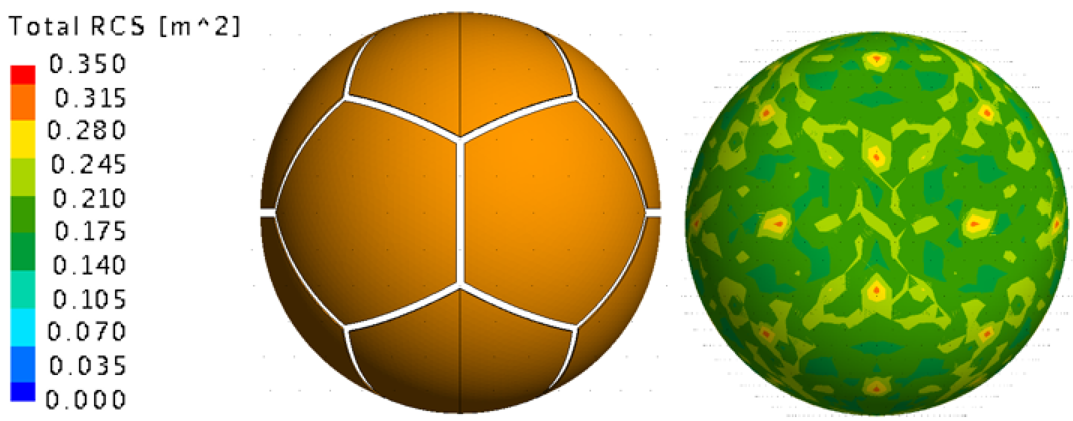

Figure 8. Monostatic RCS results of the dodecahedron in the expanded state at 3.6 GHz. The image of the target is shown on the left and its RCS simulation results on the right.

3.5 Spherical Icosahedron

Figures 9 and 10 show the monostatic RCS results for icosahedron in its contracted and expanded states, respectively. Like all of the other geometries, the icosahedron shows excellent RCS consistency over the entirety of its surface in the contracted state. In the expanded state, there are high levels of inconsistency likely due to the high number of discontinuities.

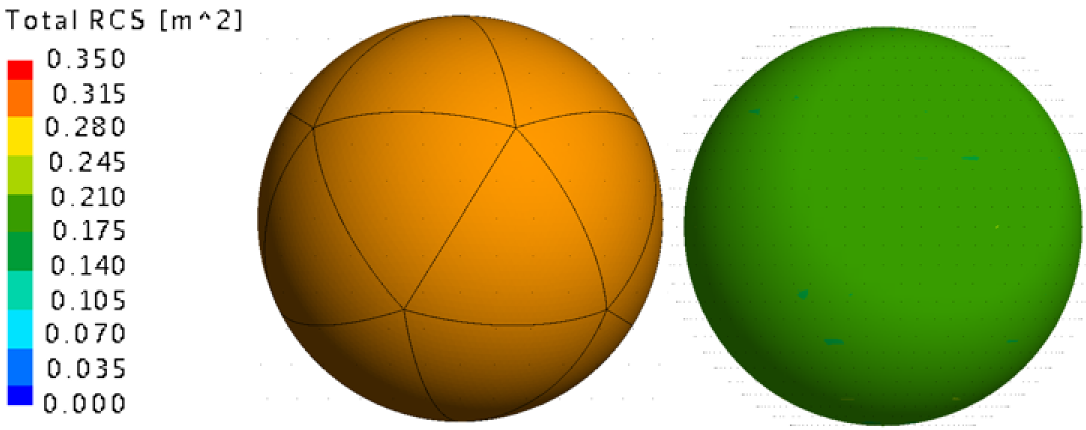

Figure 9. Monostatic RCS results of the icosahedron in the contracted state at 3.6 GHz. The image of the target is shown on the left and its RCS simulation results on the right.

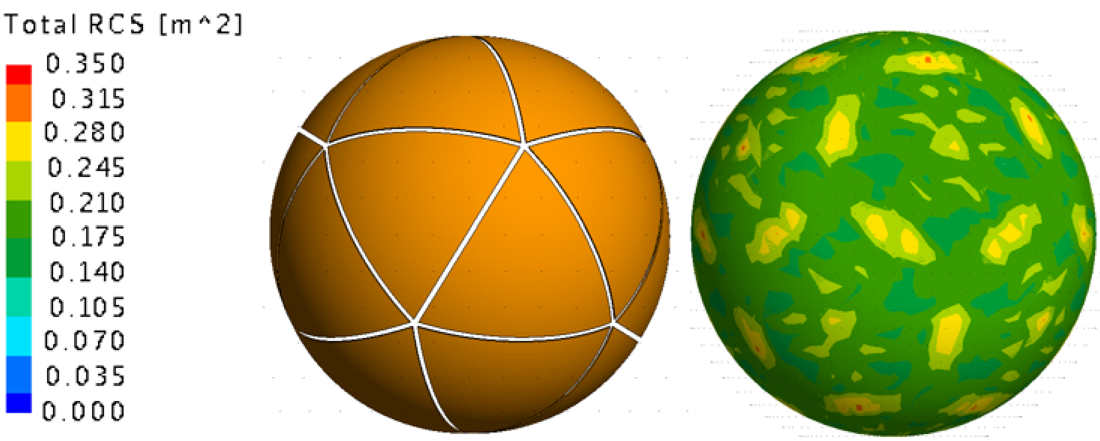

Figure 10. Monostatic RCS results of the icosahedron in the expanded state at 3.6 GHz. The image of the target is shown on the left and its RCS simulation results on the right.

3.6 Remarks

There are some common patterns and observations that can be inferred when analyzing the simulation results. The first is that our target performs exceptionally well in the contracted state for all geometries. Although there are small electrical discontinuities between faces, they are not effective enough to cause a noticeable disturbance in RCS across the surfaces of the targets. Another observation is that the RCS tends to be higher at the gaps when in the expanded state. As mentioned earlier, a hypothesis for this occurrence could be constructive interference happening when energy slips through the gaps and reflects in the specular direction back towards the radar whilst combing with energy reflected off of the target's surface. Fortunately, the change in RCS due to the gap effect is approximately 17% or 0.7 dB, and may be considered insignificant depending on the application. A third observation is that the majority of bright spots on the targets occur in the center of the faces. Although it is unclear exactly why this happens, it can be hypothesized that the spots are a product of the unique polyhedral symmetries.

Of the five geometries simulated, the octahedron is selected as the preferred dynamic calibration target. The decision is based on the following factors: scattering profile, build complexity, and spherical projection. The scattering profile is completely based on data gathered from the simulations; more specifically, the monostatic

RCS profile. The hexahedron and octahedron were the best two in this category because they showed the most RCS consistency in the expanded state. The build complexity was assessed by simplicity in mechanical design and manufacture. The fewer the moving faces, the simpler the manufacture. Therefore, polyhedra with less than eight sides pass meet this requirement. However, the variability of the RCS in the expanded state for the tetrahedron was greater than desried. Of the five geometries, the dodecahedron and icosahedron would be the most difficult to build but without a commensurate improvement in the expanded RCS compared to the other polyhedra. Our build-complexity assessment is based on our current designs to use linear actuators for each face and a control system to move each face simultaneously. Therefore, it is important that the number of faces be kept reasonably small to limit build complexity and maximize ruggedness. The last category, spherical projection, describes how well the target retains its spherical shell shape in the expanded state. For example, the tetrahedron is very poor at this because it possesses just four faces. When the four faces move radially, there appear large areas in the gaps of the target without a velocity vector towards the radar. This is in contrast to the icosahedron target, where there are twenty faces moving radially and, thus, very few areas without a velocity vector moving towards the radar. These velocity vectors are very critical for performing Doppler measurements. This criterion was the deciding factor in selecting the octahedron over the hexahedron.

4. CONCLUSION

The data presented in this paper documents the RCS signatures of five different spherical geometries. Our main objective was to find a geometry that possesses superior aspect independence at two different states: contracted and expanded. In the contracted state, all five of the geometries achieved this. The reason for this is because the target appears to the radar as a PEC sphere in this state. At 3.6 GHz, the small electrical discontinuities are not prevalent enough to prevent aspect independence. However, it was shown that the aspect independence was affected in the expanded state. The variance in RCS was minor but still present. Of the targets analyzed, the octahedron outperformed the other four geometries, that is, it had the best combination of the following traits: scattering profile, build complexity, and spherical projection.

Future plans for this work include the fabrication of a static octahedron target. RCS data will be gathered on this device and compared with simulation results. The next step will be adding a dynamic element to the device. This will be done by developing a control system consisting of linear actuators. The actuators will be used to propagate the target from a contracted state to an expanded state repeatedly. The dynamic element will allow through-wall and through-rubble Doppler testing to be performed and compared with that of a human.

5. ACKNOWLEDGMENTS

This work was supported by the National Institute of Standards and Technology (NIST) through Grant 70NANB16H023.

REFERENCES

[1] Harner, M., Narayanan, R., Brandsema, M., Jendzurski, J., and Paulter, N., "Theoretical considerations for a dynamic calibration target for through-wall and through-rubble motion-sensing doppler radar," in [*SPIE Conference on Radar Sensor Technology XXI*], Anaheim, CA, Apr. 2017, doi: 10.1117/12.2262304.

[2] Nezirovic, A., Yarovoy, A., and Ligthart, L., "Experimental study on human being detection using UWB radar," in [*2006 International Radar Symposium*], Krakow, Poland, May 2006, doi: 10.1109/IRS.2006.4338133.

[3] Nezirovic, A., Tesfay, S., Valavan, S. E., and Yarovoy, A., "Experimental study on human breathing cross section using UWB impulse radar," in [*2008 European Radar Conference*], Amsterdam, Netherlands Oct. 2008, pp. 1–4 (2008).

[4] Kumar, A., Liang, Q., Li, Z., Zhang, B., and Wu, X., "Experimental study of through-wall human being detection using ultra-wideband (UWB) radar," in [*2012 IEEE Globecom Workshops*], Anaheim, CA, pp. 1455–1459.

[5] Kiriazi, J., Boric-Lubecke, O., and Lubecke, V., "Modeling of human torso time-space characteristics for respiratory effective RCS measurements with Doppler radar," in [*2011 IEEE MTT-S International Microwave Symposium*], Baltimore, MD, Jun. 2011, doi: 10.1109/MWSYM.2011.5973284.

[6] Kiriazi, J., Boric-Lubecke, O., and Lubecke, V., "Radar cross section of human cardiopulmonary activity for recumbent subject," in [*Annual International Conference of the IEEE Engineering in Medicine and Biology Society*], Minneapolis, MN, Sep. 2009, pp. 4808–4811.

[7] Kiriazi, J., "Human cardiopulmonary recognition using close-range Doppler radar," Ph.D. dissertation, University of Hawaii, Honolulu, HI.

[8] Fryar, C., Gu, Q., and Ogden, C., "Anthropometric reference data for children and adults: United states," in [*Vital and Health Statistics. Series 11, Data from the National Health Survey*], (2007-2010).

[9] Balanis, C. A., [*Advanced Engineering Electromagnetics*], New York, NY: John Wiley & Sons (2012).